International Journal of Chemical Studies

P-ISSN: 2349–8528
E-ISSN: 2321–4902
www.chemijournal.com
IJCS 2023; 11(1): 55-62

Received: 09-10-2022
Accepted: 13-12-2022

Aphouet A Koffi
Labotatoire de Chimie-Physique, Université Félix Houphouët-Boigny, Abidjan-Cocody, 22 B.P. 582 Abidjan 22 Côte d'ivoire

Ehouman Ahissan Donatien
02 BP 802 Abidjan 02, University Nangui Abrogoua, Côte d'Ivoire.

Evrard Ablo
Labotatoire de Chimie-Physique, Université Félix Houphouët-Boigny, Abidjan-Cocody, 22 B.P. 582 Abidjan 22 Côte d'ivoire

Dje N'guessan Joel
Labotatoire de Chimie-Physique, Université Félix Houphouët-Boigny, Abidjan-Cocody, 22 B.P. 582 Abidjan 22 Côte d'ivoire

PM Niamien
Labotatoire de Chimie-Physique, Université Félix Houphouët-Boigny, Abidjan-Cocody, 22 B.P. 582 Abidjan 22 Côte d'ivoire

Siomenan Coulibali
Labotatoire de Chimie-Physique, Université Félix Houphouët-Boigny, Abidjan-Cocody, 22 B.P. 582 Abidjan 22 Côte d'ivoire

A Trokourey
Labotatoire de Chimie-Physique, Université Félix Houphouët-Boigny, Abidjan-Cocody, 22 B.P. 582 Abidjan 22 Côte d'ivoire

Corresponding Author:
Aphouet A Koffi
Labotatoire de Chimie-Physique, Université Félix Houphouët-Boigny, Abidjan-Cocody, 22 B.P. 582 Abidjan 22 Côte d'ivoire

Experimental and theoretical studies of the corrosion inhibition properties of 2-(4-chlorobenzylthio)-3-nitroH-imidazo [1, 2-α] pyridine (AE_{25}) on aluminum in 1 M hydrochloric acid medium

Aphouet A Koffi, Ehouman Ahissan Donatien, Evrard Ablo, Dje N'guessan Joel, PM Niamien, Siomenan Coulibali and A Trokourey

Abstract
Corrosion inhibition of aluminum in hydrochloric acid solution 1M by 2-(4-chlorobenzylthio)-3-nitroH-imidazo [1, 2-a] pyridine was investigated with gravimetric method and density functional theory (DFT). The experimental results revealed that 2-(4-chlorobenzylthio)-3-nitroH-imidazo [1, 2-a] pyridine (AE_{25}) has a maximum inhibition effectiveness of 99.9%. The drop in corrosion rate increases with raising concentration of AE_{25}. Studies were also performed with varying temperatures. Thermodynamic parameters calculated suggest a mixed adsorption mechanism (physisorption and chemisorption) of AE_{25} and its inhibitive action follows the modified Langmuir model ($R^2 > 0.9995$). Moreover, the standard free energy of adsorption process (ΔG°_{ads}) is negative, thus describing a spontaneous adsorption process. Also, positive values of standard enthalpy (ΔH°_{ads}) indicate that adsorption process follows an endothermic process which could be due to chemisorption. Quantum chemical calculations supported physical and chemical adsorption of AE_{25} species on the substrate.

Keywords: Corrosion inhibition; 2-(4-chlorobenzylthio)-3-nitroH-imidazo [1, 2-a] pyridine (AE_{25}); aluminium; hydrochloric acid; weight loss method; DFT

Introduction
Industrial plants are mainly made of metals and their alloys. Over time, deterioration of these material and their properties is caused by corrosion. This phenomenon resulting from a chemical or electrochemical action of the environment affects all materials, but the degeneration of metallic structures constitute the most striking examples of corrosive destruction [1, 2]. This is the case with aluminum and its alloys which despite its very stable oxide film is particularly sensitive to this phenomenon in an acid environment.

The consequences of corrosion are significant in industry. Indeed, stopping production, replacing corroded parts, accidents and the risks of pollution are frequent events with sometimes heavy economic effects [3, 4]. To solve corrosion-related problems the corroded part is replaced in most cases, but this method is very expensive. To prevent this phenomenon some possible means are the use of more resistant alloys, protection by coating and addition of inhibitors to the corrosive environment [5].

The use of corrosion inhibitors is an easy method to implement and constitutes the way of controlling the corrosive environment. Corrosion is one problem but fighting it without taking into account the environmental pollution is another, more serious one. Thus, the new European directives concerning industrial discharges are increasingly strict in terms of ecology. Development of eco-compatible and biodegradable corrosion inhibitors is now becoming a key issue.

In this context of research on green corrosion inhibitors for aluminum in a hydrochloric acid (HCl) medium that the molecule of 2-(4-chlorobenzylthio)-3-nitroH-imidazo [1, 2-a] pyridine, synthesized by E. Ablo *et al*. [6] will be explored for the first time.

2. Material and methods

2.1. Preparation of aluminum samples

Aluminum rod of 3 mm in diameter and 99.6% in purity is cut into 1 cm high. These samples are pretreated to remove any impurity. This pretreatment consisted of polishing them with abrasive paper, washing them with acetone solution then rinsing with distilled water; finally drying them in an oven at 70 °C for 10 minutes.

2.2. Synthesis of AE_{25} inhibitor

The organic molecule studied is 2-(4-clorobenzylthio)-3-nitroH-imidazo [1, 2-a] pyridine with chemical formula $C_{14}H_{10}ClN_3O_2S$ and molar mass Ma = 320 g/mol, whose synthesis [6] is summarized below.

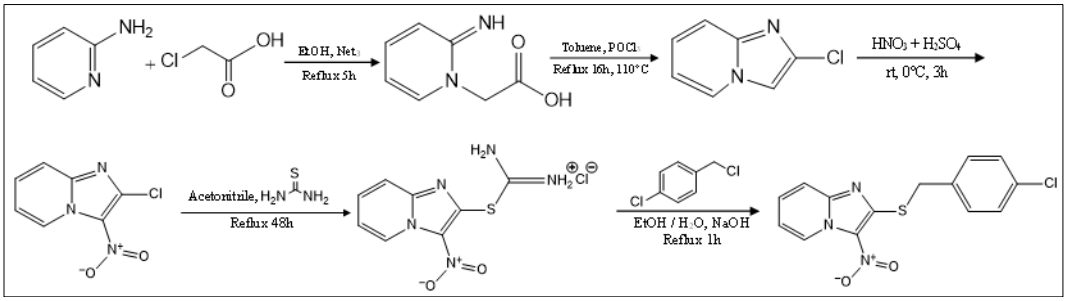

Scheme 1: Synthesis of 2-(4-clorobenzylthio)-3-nitroH-imidazo [1, 2-a] pyridine (AE_{25})

2.3. Electrolyte medium

The aluminum samples were immersed in a 1M hydrochloric acid solution without or with 2-(4-chlorobenzylthio)-3-nitroH-imidazo [1, 2-a] pyridine. Inhibitor concentrations vary between 10^{-4} and 5.10^{-3} M.

2.4. Experimental method: Gravimetry

Gravimetry consists in evaluating the mass loss undergone by a sample after being in a corrosive environment. Its results are comparable to those obtained with other methods (electrochemical, thermometric, spectroscopy, etc.) [7]. The procedure boils down to weighing the sample before and after its immersion in the study medium. The immersion time was one hour (1h), and the mass loss (Δm) undergone by the aluminium sample made it possible to calculate its corrosion rate and the inhibitory efficiency of the molecule studied.

Thus, the corrosion rate (W) and the inhibitory efficiency (IE) were obtained using the equations below:

$$W\ (mg.cm^{-2}h^{-1}) = \frac{\Delta m}{S.t} \quad (1)$$

$$IE(\%) = \frac{W_0 - W}{W_0} \times 100 \quad (2)$$

W_0 and W correspond to the corrosion rates in the absence and presence of inhibitor respectively. The corrosion rate value is the average of three tests performed under the same conditions.

2.5. Theoretical analysis by the Density Functional theory Calculations (DFT)

In order to further understand the mode of action of 2-(4-chlorobenzylthio)-3-nitroH-imidazo [1, 2-a] pyridine, its structure and electronic properties were analysed using Density Functional Theory (DFT). Theoretical parameters such as the energies of frontier molecular orbitals (E_{HOMO} and E_{LUMO}), dipole moment (μ), total energy (E_T) and Mulliken charges were determined using the Gaussian package 09W and the exchange correlation function B3LYP of Lee, Yang and Parr associated with the basic set 6-31G(d). The graphical interface used to visualize the optimized structure and molecular orbitals is Gauss View 5.0.8 [8 – 11].

According to molecular orbital theory, chemical reactivity is function of interactions between the frontier molecular orbitals, namely the Highest Occupied Molecular Orbital (HOMO) and the Lowest Unoccupied Molecular Orbital (LUMO). Indeed, the HOMO energy (E_{HOMO}) is associated with the ability of the molecule to donate electrons to a suitable acceptor with empty orbitals and the LUMO energy (E_{LUMO}) indicates its ability to accept electrons. For instance, vacant p – orbital of aluminum can accept electrons from the HOMO of the inhibitor species while it in turn donates its 3s electrons to the LUMO of the inhibitor [12].

The energy gap ΔE between the two orbitals favoring the molecule/metal interaction, is calculated with the following expression:

$$\Delta E = E_{LUMO} - E_{HOMO} \quad (3)$$

The dipole moment (μ) is an indicator of electrons distribution in the molecule and is one of the properties used to discuss and rationalize molecular structure. However, there is disagreement in the literature regarding the correlation between this parameter and inhibitory efficacy [13, 14].

Absolute hardness (η) is an important property that measures both stability and reactivity of a molecule while softness (S) is the inverse of hardness. Also, a hard entity has a high gap value (ΔE) unlike a soft entity, which makes it generally less reactive than the second. These two parameters can be calculated from the frontier orbital energies [8, 15]:

$$\eta = -\frac{E_{HOMO} - E_{LUMO}}{2} \quad (4)$$

$$S = \frac{1}{\eta} \quad (5)$$

The fraction of transferred electrons (ΔN) can be expressed by the following equation:

$$\Delta N = \frac{\chi_{Al} - \chi_{inh}}{2(\eta_{Al} + \eta_{inh})} \quad (6)$$

χ_{Al} and χ_{inh} represent the absolute electro negativities of aluminum and inhibitor respectively. However, the use of χ_{Al} is conceptually wrong here. Therefore, the metal work function $\Phi_{Al} = 4.28\ eV$ is rather used [16]. $\eta_{Al} = 0\ eV$ eV [17, 18] and η_{inh} are the respective hardness's. Thus, the fraction of electrons transferred is estimated by the new equation below:

$$\Delta N = \frac{\Phi_{Al} - \chi_{inh}}{2\eta_{inh}} \quad (7)$$

The electrophilicity index (ω) measures the propensity of chemical species to accept electrons; a high value describes a good electrophile while a small value characterizes a good nucleophile [19]. This parameter is given by the equation (8):

$$\omega = \frac{\chi^2}{2\eta} \quad (8)$$

Fukui functions are a tool for analyzing the selective reactivity of a molecule. In fact, an addition of electron will increase the electron density in a heterogeneous way; the most electrophilic sites will be more enriched. Similarly, during the withdrawal of electron the most nucleophilic areas in particular will be depleted. This reasoning leads to interest in the derivative of the electron density $\rho(\vec{r})$ with respect to the number of electrons N in the molecule. Thus, we can define the Fukui function relating to the electrophilic nature of a molecule as follows:

$$f^+(\vec{r}) = \left(\frac{\partial\rho(\vec{r})}{\partial N}\right)_{v(\vec{r}),N\geq N_0} \quad (9)$$

The Fukui function relating to the nucleophilic character is obtained from the following equation:

$$f^-(\vec{r}) = \left(\frac{\partial\rho(\vec{r})}{\partial N}\right)_{v(\vec{r}),N\leq N_0} \quad (10)$$

$v(\vec{r})$ is the external potential in which electrons move and N_0 the initial number of electrons in the molecule. The electrophilic and nucleophilic regions of a molecule are generally distinct. Hence, information provided by these two functions can be combined into a single parameter, called dual descriptor Δf_k representative of the reactivity of the molecule, positive in the electrophilic zones and negative in the nucleophilic one [10, 16].

$$\Delta f_k = \left(\frac{\partial^2\rho(\vec{r})}{\partial N^2}\right)_{v(\vec{r})} \approx f^+(\vec{r}) - f^-(\vec{r}) \quad (11)$$

Electron density is in practice calculated at fixed geometry, after addition or removal of an electron from the system. Fukui's functions can be rewritten, for each k atom of a molecule:

$$f^+(\vec{r}) = q_k(N+1) - q_k(N) \quad (12)$$

$$f^-(\vec{r}) = q_k(N) - q_k(N+1) \quad (13)$$

$q_k(N)$, $q_k(N+1)$, and $q_k(N+1)$ are Mulliken charge of k atom in the neutral, anionic and cationic system, respectively.

3. Results and discussion

3.1. Investigation by gravimetric method

3.1.1. Aluminum corrosion rate and inhibitory effectiveness of AE_{25}

The corrosion rate of aluminum in 1 M HCl solution is shown in Figure 1. In uninhibited acid medium, the rate of dissolution of the metal at room temperature (303 K) is 0.01850 g.cm^{-2}h^{-1}. This dissolution is accentuated by a rise in temperature, which could be explained by an increase in thermal agitation **[20]**, bringing its value to 0.0618 g.cm^{-2}h^{-1} at 313 K, then to 0.0845 g.cm^{-2}h^{-1} at 323K.

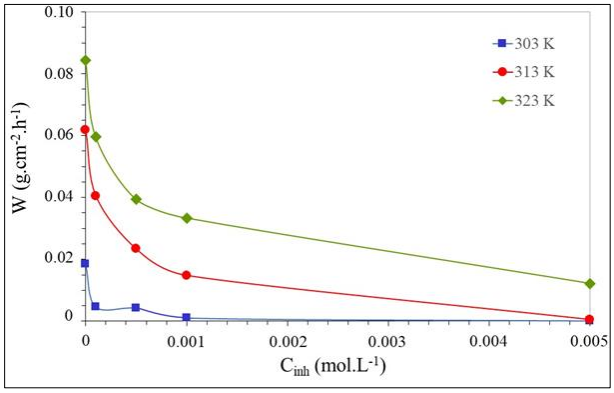

Fig 1: Corrosion rate of aluminium in 1 M HCl solution versus AE_{25} concentration at various temperatures.

However, the addition of AE_{25} in the acid solution causes this corrosion rate to drop considerably. For example, at T = 303 K and for the maximum concentration of AE_{25} (0.005 mol.L^{-1}), the corrosion rate decreases from 0.0185 g.cm^{-2}h^{-1} to 0.0001 g.cm^{-2}h^{-1}, clearly indicating the inhibiting properties of AE_{25} on the corrosion of aluminum in a 1M hydrochloric acid medium. The anticorrosive action of AE_{25} is favored by the adsorption of inhibitory species on the surface of aluminum [21 - 23]. As the concentration of AE_{25} increases, the corrosion rate decreases. This would be due to a strengthening of the inhibitory barrier formed by the adsorbed inhibitors [24].

The inhibitory efficacy of AE_{25} was plotted as a function of inhibitor concentration and temperature (Figure 2). The analysis of this figure shows that the inhibition rate increases with the concentration of inhibitor, reaching the value of 99.41% at room temperature. This performance of AE_{25} decreases when the temperature of the corrosive medium rises. Nevertheless, the value of 85.57% at 323 K is very satisfactory. According to the literature [25 - 27], the decrease in inhibitory effectiveness could be attributed to the desorption of some inhibitors from the metal surface due to thermal agitation. Moreover, the inhibition efficiency is not in proportion to the concentration of inhibitors suggesting that the species adsorb on the active sites of the substrate and form an inhibiting film.

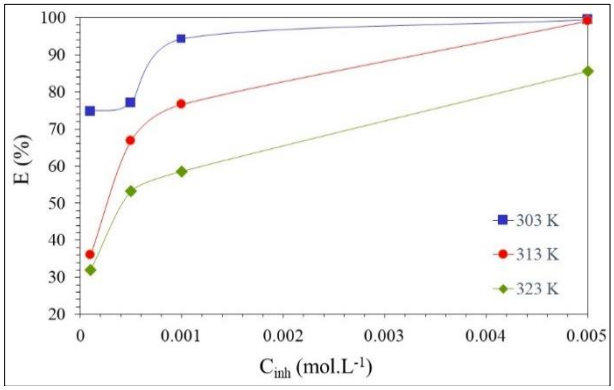

Fig 2: Inhibition efficiency versus concentration of AE_{25} in 1 M HCl solution at various temperatures

3.1.2. Adsorption isotherms and thermodynamic adsorption properties

The nature of the interactions involved in the adsorption of inhibitory species was examined using several models (Langmuir, El-Awady, Freundlich, Temkin and Dubinin-Radushkevich isotherms). For the Langmuir model, the

surface coverage (θ) and the inhibitor concentration (C_{inh}) have the following relationship:

$$\frac{C_{inh}}{\theta} = \frac{1}{K_{ads}} + C_{inh} \quad (14)$$

The graph of C_{inh}/θ versus C_{inh} is shown in Figure 3. Straight lines with correlation coefficients very close to unity are obtained indicating that Langmuir isotherm is most suitable to describe the interactions occuring at the inhibitor/metal interface. However, the slight deviation from unity observed at the slope reveals that there are interactions between species adsorbed on the metal surface and the adsorption energy varies with the increase in the surface coverage, which disagrees with the assumptions used to draw this model [28, 29]. These interactions are due to heteroatoms (Cl, S, N and O) and π bonds of the AE_{25} molecule. To take the deviation into account, the corrected Langmuir model (Villamil model) with the following equation will be considered:

$$\frac{C_{inh}}{\theta} = \frac{n}{K_{ads}} + n\, C_{inh} \quad (15)$$

The slope (n) and the intercept ($\frac{n}{K_{ads}}$) were used to calculate the adsorption equilibrium constantK_{ads}. In turn, the values of K_{ads} allowed to determine the thermodynamic parameters.

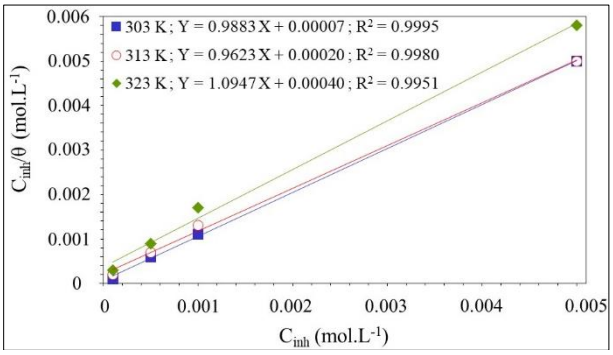

Fig 3: Plot of Langmuir adsorption isotherm of AE_{25} on aluminium in 1 M HCL solution at 303 – 323 K

The Gibbs free energy of adsorption (ΔG^0_{ads}) is calculated according to Equation (16):

$$\Delta G^0_{ads} = -RTLn(55{,}5\, K_{ads}) \quad (16)$$

55.5 (in mol.L^{-1}) is the concentration of water **[30]**; R the perfect gas constant and T the absolute temperature. The adsorption enthalpy and entropy (ΔH^o_{ads} and ΔS^o_{ads}) can be obtained by using the equation below:

$$\ln K_{ads} = \frac{-\Delta H^0_{ads}}{RT} + \frac{\Delta S^0_{ads}}{R} - lnC_{H_2O} \quad (17)$$

Figure 4 represents the plot of lnK_{ads} against the temperature giving straigtht line with slope $-\Delta H^{\circ}_{ads}/R$ and intercept$-\Delta S^{\circ}_{ads}/R - ln55.5$. The values obtained are all given in Table 1.

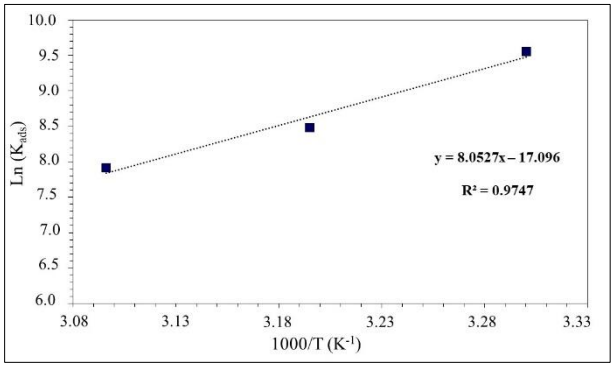

Fig 4: Plot of LnK_{ads} versus $1000/T$

The negative sign of ΔG^o_{ads} points out the spontaneity of the adsorption process of the studied inhibitor on the aluminum surface. According to the literature [31, 32], values of ΔG^0_{ads} greater than - 20 kJ.mol^{-1} reflect the existence of physisorption, while those around – 40 kJ.mol^{-1} are associated to chemisorption. In our case, the values of ΔG^0_{ads} indicate the presence of both physical and chemical adsorption.

Table 1: Thermodynamic parameters of adsorption

T (K)	K_{ads} (L.mol^{-1})	$-\Delta G^o_{ads}$ (kJ.mol^{-1})	ΔH^o_{ads} (kJ.mol^{-1})	ΔS^o_{ads} (J.mol^{-1}.K^{-1})
303	14118.57	34.174	- 66.918	-108.69
313	4811.50	32.500		
323	2736.75	32.024		

Moreover, the value of ΔH^0_{ads} is negative showing that the adsorption of the inbibitor follows an exothermic process. In addition, $\Delta S^0_{ads} < 0$ indicates a decrease in disorder during the adsorption of the inhibitor.

3.1.3. Evaluation of kinetic parameters

Thermodynamic activation parameters like apparent activation energy (E^*_a), enthalpy (ΔH^*_a) and entropy (ΔS^*_a) of activation give important information about corrosion inhibition mechanism [33, 34]. The corrosion's process activation energy can be determined by the Arrhenius equation below:

$$\log W = \frac{-E^*_a}{2{,}303RT} + logA \quad (18)$$

Where A is the Arrhenius pre-exponential factor. The plot of $logW$ versus $1000/T$ (Figure 5) is a straight line with a slope equivalent to$-E^*_a/2{,}303R$. Activation energy (E^*_a) values are calculated from the slopes of these linear lines and summarized in Table 2. As seen in this table, the results obtained in the presence of AE_{25}, $E^*_a(inh)$, showed higher values than those without. Aluminium dissolution becomes harder due to a physical barrier formed by the inhibitor on the substrate. The energy increases when the concentration of inhibitor raises, thus favoring the formation of electrostatic bonds.

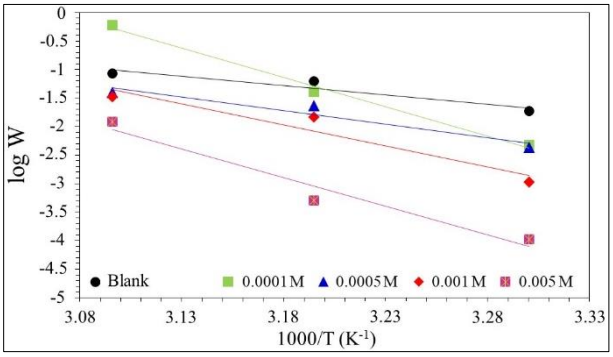

Fig 5: Plot of log W versus 1000/T for aluminum in 1 M HCl without or with AE_{25}

Table 2: Activation parameters of aluminum immersed in 1 M HCl without or with inhibitor

C_{inh} (mol.L^{-1})	E_a^* (kJ.mol^{-1})	ΔH_a^* (kJ.mol^{-1})	ΔS_a^* (J.mol^{-1}K^{-1})
0	62.106	59.507	314.389
1.10^{-4}	196.833	194.230	745.541
5.10^{-4}	91.070	88.470	398.111
1.10^{-3}	140.922	138.323	551.923
5.10^{-3}	192.087	189.494	696.969

The enthalpy (ΔH_a^*) and entropy (ΔS_a^*) of activation for aluminium dissolution are evaluated using the following transition state equation:

$$W = \frac{R.T}{\aleph.h} exp\left(\frac{\Delta S_a^*}{R}\right).exp\left(-\frac{\Delta H_a^*}{R.T}\right) \quad (19)$$

Where $\aleph$ (mol^{-1}) is the Avogadro's number and h (J. s^{-1}) the Planck's constant. The graph of $log\, W/T$ versus $1000/T$ for aluminium in 1 M HCl with various concentrations of AE_{25} is presented in Figure 6 below. The values of ΔH_a^* and ΔS_a^* calculated from the slope and intercept are given in the previous table. The positive values of ΔH_a^* reflected the endothermic process of the aluminum dissolution. $\Delta S_a^* > 0$ suggested an increase in disorder during the dissolution of aluminum, which could explain the decrease in inhibitory efficiency with the rise in temperature.

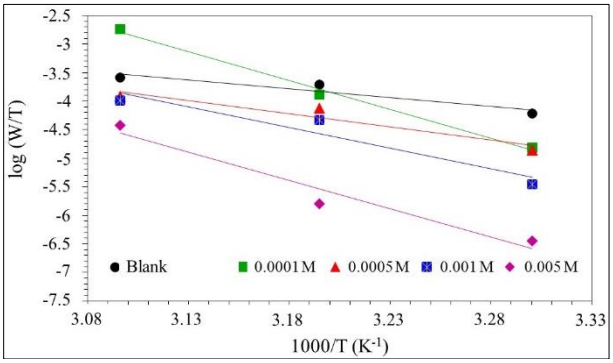

Fig 6: Plot of log (W/T) versus 1000/T for aluminum in 1 M HCl without or with AE_{25}

3.2. Theoretical study of the inhibition

3.2.1. Global Reactivity Descriptors

The global descriptors mentioned above were determined and summarized in Table 3. The value of the number of transferred electrons (ΔN) shows how electrons are transferred during the inhibition process. According to the literature [35, 36], $\Delta N > 0$ indicates that the inhibitor is an electron donor whilst it is an electron acceptor if < 0. It is also reported that $\Delta N < 3.6$ suggests an increase in inhibition efficiency with increasing ability to donate electrons to a metal surface. In this study, the negative value of ΔN shows that AE_{25} cannot yield electrons to the aluminum surface, however, it receive some. The high value of the electrophilicity index ($\omega = 4.576\, eV$) confirms this electrophilic property of the molecule studied [18].

According to molecular orbital theory, the energy of LUMO suggests a greater probability for a molecule to accept electrons. Thus, a lower value of E_{LUMO} indicates an improvement in adsorption of inhibitor on the metal surface, and with lower ΔE the inhibitor is of stronger adsorptive ability [37]. In this study, $E_{LUMO} = -2{,}280$ eV and $\Delta E = 4.059$ eV are low compared to the literature [37, 38]. Therefore, the AE_{25} molecule could receive electrons from the metal to form back-donating bond sustaining the existence of chemisorption and consequently a better inhibition efficiency.

The two frontier orbits of the highest occupied molecular orbital (HOMO) and the lowest unoccupied molecular orbital (LUMO) were shown in Figure 7. Both HOMO and LUMO lobes are located on the pyridine ring. LUMO electron density is particularly distributed over O, N and S heteroatoms that could constitute the possible binding sites of electrophilic attack.

Table 3: Quantum Chemical Parameters of AE_{25} calculated using B3LYP/6-31G (d)

E_{HOMO} (eV)	E_{LUMO} (eV)	ΔE (eV)	μ (D)	E_T (Ha)	χ (eV)	η (eV)	S (eV^{-1})	ω (eV)	ΔN
-6.340	-2.280	4.059	6.767	-1712.505	4.310	2.030	0.493	4.576	-0.007

It is further reported that the dipole moment of a chemical species can be related to the strength of adsorption [13, 38]. In our case, its value is quite high showing a strong adsorption of AE_{25} on the aluminum surface, which could justify the excellent inhibition rate obtained.

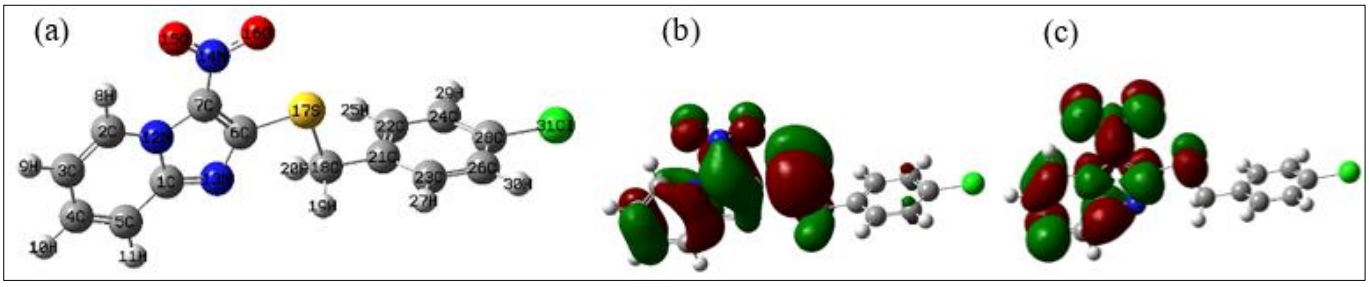

Fig 7: (a) Optimized structure; (b) HOMO and (c) LUMO of AE_{25}

3.2.2. Local Reactivity Descriptors

The local reactivity of the inhibitor was analyzed through Fukui functions and the dual descriptor. The parameters were calculated using Mulliken atomic charge for neutral, cationic and anionic AE_{25} species and reported in Table 4. The maximum values of f_k^+ and f_k^- represent the preferred sites for attack by a nucleophile and an electrophile respectively. Moreover, the most negative value of Δf_k indicate that the site may be favored for an electrophilic attack, while the expected site for a nucleophilic attack is indicated by the most positive value of Δf_k. According to Table 4, C1 and C7 atoms are the preferred sites for nucleophilic attacks, whereas electrophilic attack would preferably occur at N13 atom. Otherwise, the oxygen atom (O16) has a low Fukui dual function ($\Delta f_k = -0.088635$) and could also be an electrophilic site. These findings are in good agreement with the theory of frontier orbitals, namely LUMO and HOMO.

Table 4: Mulliken charges, Fukui functions and dual descriptor of AE_{25} by B3LYP/6-31G (d)

Atom N°	$q_k(N+1)$	$q_k(N)$	$q_k(N-1)$	f_k^+	f_k^-	Δf_k
C1	0.504990	0.543843	0.651062	-0.038853	-0.107219	0.068366
C2	0.052509	0.074714	0.094919	-0.022205	-0.020205	-0.002000
C3	-0.198507	-0.190135	-0.174116	-0.008372	-0.016019	0.007647
C4	-0.149236	-0.105163	-0.089544	-0.044073	-0.015619	-0.028454
C5	-0.188052	-0.178737	-0.160623	-0.009315	-0.018114	0.008799
C6	0.003783	0.05971	0.150613	-0.055927	-0.090903	0.034976
C7	0.518893	0.473483	0.452890	0.045410	0.020593	0.024817
H8	0.196878	0.231620	0.276000	-0.034742	-0.044380	0.009638
H9	0.099526	0.163258	0.219679	-0.063732	-0.056421	-0.007311
H10	0.088213	0.158826	0.216861	-0.070613	-0.058035	-0.012578
H11	0.108765	0.169709	0.209117	-0.060944	-0.039408	-0.021536
N12	-0.568532	-0.548573	-0.566591	-0.019959	0.018018	-0.037977
N13	-0.57557	-0.548283	-0.717195	-0.027287	0.168912	-0.196199
N14	0.209443	0.336758	0.382991	-0.127315	-0.046233	-0.081082
O15	-0.578872	-0.448804	-0.397968	-0.130068	-0.050836	-0.079232
O16	-0.544477	-0.410897	-0.365952	-0.133580	-0.044945	-0.088635
S17	0.173371	0.238593	0.372691	-0.065222	-0.134098	0.068876
C18	-0.501267	-0.510652	-0.570041	0.009385	0.059389	-0.050004
H19	0.178096	0.201000	0.203138	-0.022904	-0.002138	-0.020766
H20	0.178044	0.201068	0.203170	-0.023024	-0.002102	-0.020922
C21	0.158789	0.142537	0.130877	0.016252	0.01166	0.004592
C22	-0.162297	-0.159212	-0.153296	-0.003085	-0.005916	0.002831
C23	-0.162269	-0.159227	-0.153273	-0.003042	-0.005954	0.002912
C24	-0.132077	-0.128484	-0.125256	-0.003593	-0.003228	-0.000365
H25	0.139067	0.144473	0.151346	-0.005406	-0.006873	0.001467
C26	-0.132084	-0.128471	-0.125258	-0.003613	-0.003213	-0.000400
H27	0.139097	0.144469	0.151336	-0.005372	-0.006867	0.001495
C28	-0.064637	-0.064096	-0.062412	-0.000541	-0.001684	0.001143
H29	0.137976	0.158793	0.182858	-0.020817	-0.024065	0.003248
H30	0.137982	0.158793	0.182858	-0.020811	-0.024065	0.003254
Cl31	-0.067546	-0.020914	0.034838	-0.046632	-0.055752	0.009120

3.3. Mechanism of corrosion inhibition

It is well know that inhibitors in HCl solution are found in their neutral form or as protonated cations. Moreover, corrosion inhibition of aluminium in acid medium occurs by adsorption of the inhibitors onto the metal surface depending on the charge of the surface and the chemical structure of the inhibitor. Indeed, physical adsorption requires an electrically charged metal surface (by chloride ions or metal ions Al^{3+}) and charged species in the solution (especially inhibitor cations). Chemical adsorption can occur by sharing electrons through "donor-acceptor" bonds between aluminum and the molecule studied. Accordingly, several inhibition mechanisms can be proposed in this study, including the protonation of 2-(4-chlorobenzylthio)-3-nitroH-imidazo [1, 2-α] pyridine.

The energy gap of AE_{25} ($\Delta E = 4.059\ eV$) is low indicating that this molecule is very reactive such that it could easily be protonized in the medium or form a metal complex. Protonation (Equation 20) can occur through heteroatoms, especially the nitrogen atom and nitro group, according to the results of the local reactivity study. Figure 8 below shows two protonated form of AE_{25}. Otherwise, AE_{25} could react with Al^{3+} ions released in the acid medium to form metal complex (Equation 21), which would adsorb on the substrate [40].

$$[AE_{25}] + x\ H^+ \rightarrow [AE_{25}H_x]^{x+} \quad (20)$$

$$[AE_{25}] + Al^{3+} \rightarrow [AE_{25} - Al]^{3+} \quad (21)$$

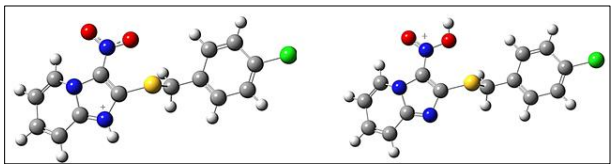

Fig 8: Protonated forms of AE_{25} in 1M HCl acid medium

The cations formed get adsorbed on the aluminum surface previously charged with chloride ions (Cl^-). Indeed, the anodic site of aluminium surface is first charged with metal ions (Al^{3+}) [41] in a 1M hydrochloric acid medium. Then, the chloride ions physically interact with this positively charged surface. The cationic species, $[AE_{25} - Al]^{3+}$, can also be

adsorbed at the cathodic sites on the aluminum surface in competition with H^+ ions reducing the rate of hydrogen evolution [42]. The interactions between charged inhibitors and the aluminum surface are electrostatic in nature [43].

Besides the cationic species, the AE_{25} molecules can replace the water molecules previously adsorbed according to Equation 22. The neutral inhibitor could receive electrons from aluminium surface to form back-donating bond. This adsorption occur chemically and may explain the high inhibitory efficacy obtained at 30 °C [43].

$$Inh_{(sol)} + n\,H_2O_{ads} \rightarrow Inh_{ads} + n\,H_2O_{(sol)} \qquad (22)$$

4. Conclusion

The newly synthetized 2-(4-chlorobenzylthio)-3-nitroH-imidazo [1, 2-α] pyridine, (AE_{25}), provides excellent protection for aluminum in acid medium. Inhibition efficiency increases as the concentration of inhibitory species increases from 10^{-4} M to 5.10^{-3} M. The maximum efficacy of 99.43% was reached for a concentration of 5.10^{-3} M at 303 K. The thermodynamics parameters indicated that AE_{25} species were adsorbed physically and chemically on the aluminum surface with a predominance of physisorption. The adsorption follows the modified Langmuir model (Villamil model), so there are interactions between adsorbed species and an inhibitor is adsorbed on several active sites of the metal.

Theoretical calculations corroborate those of the gravimetric method since the value of ΔN confirms the physisorption which is preponderant in the process of adsorption of the inhibitor on the substrate. DFT also showed that the HOMO and LUMO localized around 2-thio, 3-nitroH-imidazo [1, 2-α] pyridine contain the electrophilic (C1 and C7 atoms) and nucleophilic (N13 and O16 atoms) sites.

Conflicts of interest

There are no conflicts to declare.

References

1. Kain V. Corrosion: Resistant Materials, in: S. Banerjee and A. Tyagi (Eds.), Functional
2. Materials Preparation, Processing and Applications, Elsevier, London, USA, 2012, 507–547. ISBN: 978-0-12-385142-0.
3. Plieth W. Corrosion and Corrosion Protection, in: Electrochemistry for Materials Science. Elsevier. 2008, 291-321, ISBN: 978-0-444-52792-9.
4. Brossia CS. Laboratory Assessment of Corrosion, in: M. Kutz (Ed.), Handbook of Environmental Degradation of Materials (Second Edition), Elsevier, 2012, 33-62. ISBN: 978-1-4377-3455-3**.**
5. Solmaz R, Şahin EA, Döner A, Kardaş G. The investigation of synergistic inhibition effect of rhodanine and iodide ion on the corrosion of copper in sulphuric acid solution, Corros. Sci. 2011;53(10):3231-3240.
6. Sastri VS. Green Corrosion Inhibitors: Theory and Practice (First Edition), John Wiley & Sons, 2011. DOI: 10.1002/9781118015438.
7. Evrard Ablo, Siomenan Coulibali, Daouda Touré, Souleymane Coulibaly, Ahmont Landry Claude Kablan, Fernique Konan Kouadio, Drissa Sissouma, Nathalie Guessend Kouadio & Adjou Ané, Synthesis and antibacterial activity *in vitro* of 2-benzylthioimidazo [1,2-a] pyridine derivatives against pathogenic bacterial, Synthetic Communications, 2022. DOI: 10.1080/00397911.2022.2032175.
8. El Naggar M. Corrosion inhibition of mild steel in acidic medium by some sulfa drugs compounds, Corros. Sci. 2007;49:2236-2236.
9. Burak Tüzün, Jeetendra Bhawsar, Quantum chemical study of thiaozole derivatives as corrosion inhibitors based on density functional theory, Arabian Journal of Chemistry. 2021;14:102927.
10. Kun Cao, Wenheng Huang, Xi Huang and Jie Pan, Imidazo [1,2-a] Pyrimidine Derivatives as Effective Inhibitor of Mild Steel Corrosion in HCl Solution: Experimental and Theoretical Studies, Frontiers in Materials. 2022 March;9(843522):1-16.
11. Oluwatoba Emmanuel Oyeneyin, Nathanael Damilare Ojo, Nureni Ipinloju, Eric Bamidele Agbafa and Abiodun Vestor Emmanuel, Investigation of the corrosion inhibition potentials of some 2-(4-(substituted) arylidene)-1H-indene-1,3-dione derivatives: density functional theory and molecular dynamics simulation, Beni-Suef University Journal of Basic and Applied Sciences. 2022;11(132):1-14.
12. Lamia Boucherit, Tahar Douadi, Nadjib Chafai, Mousa Al-Noaimi, Salah Chafaa, The inhibition Activity of 1,10 - bis(2-formylphenyl)-1,4,7,10- tetraoxadecane (Ald) and its Schiff base (L) on the Corrosion of Carbon Steel in HCl: Experimental and Theoretical Studies, Int. J. Electrochem. Sci. 2018;13:3997-4025. doi: 10.20964/2018.04.59.
13. Beda RHB, Niamien PM, Avo Bilé EB, Trokourey A. Inhibition of Aluminium Corrosion in 1.0 M HCl by Caffeine: Experimental and DFT Studies, Advances in Chemistry. 2017;6975248:10. https://doi.org/10.1155/2017/6975248.
14. Babatunde Temitope Ogunyemi, Dayo Felix Latona, Abraham Abiodun Ayinde, Isaiah Ajibade Adejoro, Theoretical Investigation to Corrosion Inhibition Efficiency of Some Chloroquine Derivatives Using Density Functional Theory, Advanced Journal of Chemistry-Section A. 2020;3(4):485-492.
15. Ogunyemi BT, Adejoro IA. Corrosion Inhibitor Potential of Four Phenyltetrazoles Derivatives using Density Functional Theory and Quantitative Structure-Activity Equation Approach, J. Appl. Sci. Environ. Manage. 2019 April;23(4):665-671.
16. Loutfy H Madkour, Elshamy IH. Experimental and computational studies on the inhibition performances of benzimidazole and its derivatives for the corrosion of copper in nitric acid, Int J Ind Chem. 2016;7:195–221.
17. N'guessan Yao Silvère Diki, Gbe Gondo Didier Diomandé, Sagne Jacques Akpa, Augustin Ouédraogo, Lemeyonouin Aliou Guillaume Pohan, Paulin Marius Niamien and Albert Trokourey, Aluminum Corrosion Inhibition by 7-(Ethylthiobenzimidazolyl) Theophylline in 1M Hydrochloric Acid: Experimental and DFT Studies, International Journal of Applied Pharmaceutical Sciences and Research. 2018 Oct-Dec;3(4):41-53.
18. Parr RG, Pearson RG. Absolute hardness: companion parameter to absolute electronegativity, J. Am. Chem. Soc., 1983;105:7512-7516.
19. Sastri VS, Perumarddi JR. Molecular Orbital Theoretical studies of some organic corrosion inhibitors, Corros. 1997;53:617-622.
20. N'guessan Yao Silvère Diki, Nagnonta Hippolyte Coulibaly, Ollo Kambiré, Albert Trokourey, Experimental and Theoretical Investigations on Copper Corrosion Inhibition by Cefixime Drug in 1M HNO_3

Solution, Journal of Materials Science and Chemical Engineering. 2021;9:11-28.
21. Kairi NI, Kassim J. The Effect of Temperature on the Corrosion Inhibition of Mild Steel in 1 M HCl Solution by Curcuma Longa Extract, Int. J. Electrochem. Sci. 2013;8:7138-7155.
22. Kadhum AAH, Mohamad AB, Hammed LA, Al-Amiery AA, San N, Musa AY. Inhibition of Mild Steel Corrosion in Hydrochloric Acid Solution by New Coumarin, Mat. 2014;7:4335-4348.
23. Eddy NO, Odiongenyi AO, Ameh PO, Ebenso EE. Corrosion Inhibition Potential of Daniella Oliverri Gum Exudate for Mild Steel in Acidic Medium, Int. J. Electrochem. Sci. 2012;7:7425-7439.
24. Halambek J, Žutinić A, Berković K, Ocimum basilicum L. Oil as Corrosion Inhibitor for Aluminium in Hydrochloric Acid Solution, Int. J. Electrochem. Sci. 2013;8:11201-11214.
25. Oguzie, Emeka E., Corrosion Inhibitive Effect and Adsorption Behaviour of *Hibiscus Sabdariffa* Extract on Mild Steel in Acidic Media, Portugaliae Electrochemica Acta. 2008;26(3):303-314.
26. Davilal Parajuli, Srijana Sharma, Hari Bhakta Oli, Dilip Singh Bohara, Deval Prasad Bhattarai, Arjun Prasad Tiwari and Amar Prasad Yadav, Comparative Study of Corrosion Inhibition Efficacy of Alkaloid Extract of *Artemesia vulgaris* and Solanum tuberosum in Mild Steel Samples in 1 M Sulphuric Acid, Electrochem. 2022;3:416–433.
27. Kenneth Kanayo Alaneme, Sunday Joseph Olusegun, Oluwabunkunmi Tomi Adelowo, Corrosion inhibition and adsorption mechanism studies of *Hunteria umbellata* seed husk extracts on mild steel immersed in acidic solutions, Alexandria Engineering Journal. 2016;55:673-681.
28. Dongyi Li, Panpan Zhang, Xinyu Guo, Xiaowei Zhao and Ying Xu, The inhibition of mild steel corrosion in 0.5 M H_2SO_4 solution by radish leaf extract, RSC Adv. 2019;9:40997–41009.
29. Karthikaiselvi R, Subhashini S. Study of adsorption properties and inhibition of mild steel corrosion in hydrochloric acid media by water soluble composite poly (vinyl alcohol-o-methoxy aniline), Journal of the Association of Arab Universities for Basic and Applied Sciences. 2014;16:74–82.
30. Joherbson Deivid dos S. Pereira, Jannyely M Neri, Denise P. Emerenciano, Gutto Raffyson S. de Freitas, Maria Beatriz M. Cansanção Felipe, Miguel Ângelo F. de Souza, Fabrício G. Menezes and Maria Aparecida M. Maciel, Experimental and theoretical analysis of an oxazinoquinoxaline derivative for corrosion inhibition of aisi 1018 steel, Quim. Nova. 2018;41(3):243-250. http://dx.doi.org/10.21577/0100-4042.20170171.
31. N'guessan Yao Silvère Diki, Nagnonta Hippolyte Coulibaly, Kadjo François Kassi and Albert Trokourey, Mild steel corrosion inhibition by 7-(ethylthiobenzimidazolyl) theophylline, J. Electrochem. Sci. Eng. 2021;11(2):97-106.
32. Olatunde Alaba Akinbulumo, Oludare JohnsonOdejobi, Ebenezer Leke Odekanle, Thermodynamics and adsorption study of the corrosion inhibition of mild steel by *Euphorbia heterophylla L*. extract in 1.5 M HCl, Results in Materials. 2020 March;5:100074, 1-6.
33. Dewar MJS, Thiel W. Ground States of Molecules, 38. The MNDO Method. Approximations and Parameters. J. Am. Chem. Soc. 1977;99:4899-4907.
34. Farhad Mohsenifar, Hojat Jafari, Koray Sayin, Investigation of Thermodynamic Parameters for Steel Corrosion in Acidic Solution in the Presence of N, N'-Bis(phloroacetophenone)-1,2 propanediamine, J Bio Tribo Corros. 2016;2(1):1-13.
35. Gomma GK. Mechanism of corrosion behaviour of carbon steel in tartaric and malic acid in the presence of Fe^{2+} ion, Mat. Chem. phys. 1998;52:200-206.
36. Idir B, Kellou-Kerkouche F. Experimental and Theoretical Studies on Corrosion Inhibition Performance of Phenanthroline for Cast Iron in Acid Solution, J. Electrochem. Sci. Technol. 2018;9(4):260-275.
37. Szymon Malinowski, Computational Design of Anticorrosion Properties of Novel, Low-Molecular Weight Schiff Bases, Materials. 2022;15(19):6725. https://doi.org/10.3390/ma15196725
38. Nuha Ahmed Wazzan, Fatma Mohamed Mahgoub, DFT Calculations for Corrosion Inhibition of Ferrous Alloys by Pyrazolopyrimidine Derivatives, Open Journal of Physical Chemistry. 2014;4:6-14.
39. Tigori MA, Niamien PM, Yapo AJ, Trokourey A. Effect of pyridoxine hydrochloride on copper corrosion in 1M HNO_3, Journal of Chemical, Biological and Physical Sciences, Sec. C. 2016;6(4):1201-1216.
40. Salah Eddine Lemallem, Abdelali Fiala, Hayet Brahim Ladouani, and Hamza Allal, Corrosion Inhibition Performance of Two Ketene Dithioacetal Derivatives for Stainless Steel in Hydrochloric Acid Solution, J. Electrochem. Sci. Technol. 2022;13(2):237-253.
41. Deng S, Li X. Inhibition by Jasminum nudiflorum Lindl. leaves extract of the corrosion of aluminium in HCl solution, Corros. Sci. 2012;64:253–262.
42. Natishan PM, McCafferty E, Hubler GK. The Effect of pH of Zero Charge on the Pitting Potential, J. Electrochem. Soc. 1986;133(5):1061-1062.
43. Ramazan Solmaz, Investigation of corrosion inhibition mechanism and stability of Vitamin B1 on mild steel in 0,5 M HCl solution, Corros. Sci. 2014;81:75–84.
44. Faustin M, Maciuk A, Salvin P, Roos C, Lebrini M. Corrosion inhibition of C38 steel by alkaloids extract of *Geissospermum* laeve in 1 M hydrochloric acid: Electrochemical and phytochemical studies, Corros. Sci. 2015;92:287–300.